Nasbíráno 1.4.2002 pro přepsání do dvouznakového zápisu

$$S^{ij} = \begin{pmatrix} \Sigma_c^{++} & \sqrt{\frac{1}{2}}\Sigma_c^{+} & \sqrt{\frac{1}{2}}\Xi_c^{+'} \\ \sqrt{\frac{1}{2}}\Sigma_c^{+} & \Sigma_c^{0} & \sqrt{\frac{1}{2}}\Xi_c^{0'} \\ \sqrt{\frac{1}{2}}\Xi_c^{+'} & \sqrt{\frac{1}{2}}\Xi_c^{0'} & \Omega_c^{0} \end{pmatrix}$$

$$(T_1, T_2, T_3) = (\Xi_b^-, -\Xi_b^0, \Lambda_b^0) \ ,$$

$$S^{ij} = \begin{pmatrix} \Sigma_b^{+} & \sqrt{\frac{1}{2}}\Sigma_b^{0} & \sqrt{\frac{1}{2}}\Xi_b^{0'} \\ \sqrt{\frac{1}{2}}\Sigma_b^{0} & \Sigma_b^{-} & \sqrt{\frac{1}{2}}\Xi_b^{-'} \\ \sqrt{\frac{1}{2}}\Xi_b^{0'} & \sqrt{\frac{1}{2}}\Xi_b^{-'} & \Omega_b^{-} \end{pmatrix} \ .$$

c quark	b quark	μ_χ	μ_{g3}	μ_{g2}
Σ_c^{++}	Σ_b^{+}	2	$1 + m_\pi/m_K$	$I_\pi + I_K$
Σ_c^{+}	Σ_b^{0}	1/2	1/2	$I_K/2$
Σ_c^{0}	Σ_b^{-}	-1	$-m_\pi/m_K$	$-I_\pi$
$\Xi_c^{0'}$	$\Xi_b^{-'}$	-1	$-(1 + m_\pi/m_K)/2$	$-(I_\pi + I_K)/2$
$\Xi_c^{+'}$	$\Xi_b^{0'}$	1/2	$m_\pi/(2m_K)$	$I_\pi/2$
Ω_c^{0}	Ω_b^{-}	-1	-1	$-I_K$

Table 2: Contributions to magnetic moments of spin 1/2 c and b-baryons ($s_l = 1$).

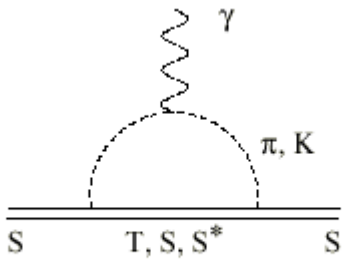

Figure 1: Meson loops contributing to S-baryons MM.

Using Table 2 one can derive the following linearly independent relations for the magnetic moments of spin 1/2 baryons containing a c-quark:

$$\begin{aligned}
\mu(\Sigma_c^{++}) + \mu(\Sigma_c^0) &= 2\mu(\Sigma_c^+) \\
\mu(\Sigma_c^{++}) + \mu(\Omega_c^0) &= 2\mu(\Xi_c^{+'}) \\
\mu(\Sigma_c^{++}) + 2\mu(\Xi_c^{0'}) &= \mu(\Sigma_c^0) + 2\mu(\Xi_c^{+'}) \\
\mu(\Sigma_c^0) + 2\mu(\Xi_c^{+'}) &= \frac{1}{6m_c} \, . \qquad (19)
\end{aligned}$$

Including the spin 3/2 baryons one can derive six more independent relations,

$$\begin{aligned}
\mu(\Sigma_c^{++*}) + \mu(\Sigma_c^{0*}) &= 2\mu(\Sigma_c^{+*}) \\
\mu(\Sigma_c^{++*}) + \mu(\Omega_c^{0*}) &= 2\mu(\Xi_c^{+'*}) \\
\mu(\Sigma_c^{++*}) + 2\mu(\Xi_c^{0'*}) &= \mu(\Sigma_c^{0*}) + 2\mu(\Xi_c^{+'*}) \\
\mu(\Sigma_c^{0*}) + 2\mu(\Xi_c^{0'*}) &= 3\left(\mu(\Sigma_c^0) + 2\mu(\Xi_c^{+'})\right) \\
\frac{2}{3}\mu(\Sigma_c^{++*}) &= \mu(\Sigma_c^0) + 2\mu(\Xi_c^{+'}) - \mu(\Sigma_c^{++}) \\
6\mu(\Sigma_c^+) - 4\mu(\Sigma_c^{++}) &= -4\mu(\Sigma_c^{+*}) + \frac{8}{3}\mu(\Sigma_c^{++*}) \, . \qquad (20)
\end{aligned}$$

$\Sigma_c^{++} + \Sigma_c^0 = 2\Sigma_c^+$

$$\Sigma_c^{++} + \Sigma_c^0 = 2\,\Sigma_c^+ \qquad \frac{x^4 \cdot t^1}{x^1 \cdot t^3} \cdot \frac{x^4 \cdot t^3}{x^1 \cdot t^5} = \frac{(x^4 \cdot t^2)^2}{(x^1 \cdot t^4)^2} \qquad 10 \;\; 12$$

$\Sigma_c^{++} + \Omega_c^0 = 2\Xi_c^+$

$$\Sigma_c^{++} + \Omega_c^0 = 2\,\Xi_c^+ \qquad \frac{x^4 \cdot t^1}{x^1 \cdot t^3} \cdot \frac{x^6 \cdot t^3}{x^3 \cdot t^5} = \frac{(x^5 \cdot t^2)^2}{(x^2 \cdot t^4)^2} \qquad \begin{matrix} 14 & 12 \\ 14 & 12 \end{matrix}$$

$\Sigma_c^{++} + 2\Xi_c^0 = \Sigma_c^0 + 2\,\Xi_c^+$

$$\Sigma_c^{++} + 2\,\Xi_c^0 = \Sigma_c^0 + 2\,\Xi_c^+ \qquad \frac{x^4 \cdot t^1}{x^1 \cdot t^3} \cdot \frac{(x^5 \cdot t^3)^2}{(x^2 \cdot t^5)^2} = \frac{x^4 \cdot t^3}{x^1 \cdot t^5} \cdot \frac{(x^5 \cdot t^2)^2}{(x^2 \cdot t^4)^2} \qquad \begin{matrix} 19 & 20 \\ 19 & 20 \end{matrix}$$

$6\,\Sigma_c^+ - 4\,\Sigma_c^0 = 4\Sigma_c^+ + 8/3\;\Sigma_c^{++}$

$$6\,\Sigma_c^+ - 4\,\Sigma_c^0 = 4\Sigma_c^+ + 8/3\;\Sigma_c^{++} \qquad \frac{(x^4 \cdot t^2)^6}{(x^1 \cdot t^4)^6} \cdot \frac{(x^1 \cdot t^5)^4}{(x^4 \cdot t^3)^4} = \frac{(x^4 \cdot t^2)^4}{(x^1 \cdot t^4)^4} \cdot \frac{(x^4 \cdot t^1)^8}{(x^1 \cdot t^3)^8} \qquad \begin{matrix} 68 & 62 \\ 40 & 72 \end{matrix}$$

The last three equations connect observables corresponding to spin 1/2 and spin 3/2 baryons.

Moreover, it is easy to deduce 10 analogous equations that relate baryons having a b-quark

$$\begin{aligned}
\mu(\Sigma_b^+) + \mu(\Sigma_b^-) &= 2\mu(\Sigma_b^0) \\
\mu(\Sigma_b^+) + \mu(\Omega_b^-) &= 2\mu(\Xi_b^{0'}) \\
\mu(\Sigma_b^+) + 2\mu(\Xi_b^{-'}) &= \mu(\Sigma_b^-) + 2\mu(\Xi_b^{0'}) \\
\mu(\Sigma_b^-) + 2\mu(\Xi_b^{0'}) &= -\frac{1}{12m_b} \\
\mu(\Sigma_b^{+*}) + \mu(\Sigma_b^{-*}) &= 2\mu(\Sigma_b^{0*}) \\
\mu(\Sigma_b^{+*}) + \mu(\Omega_b^{-*}) &= 2\mu(\Xi_b^{0'*}) \\
\mu(\Sigma_b^{+*}) + 2\mu(\Xi_b^{-'*}) &= \mu(\Sigma_b^{-*}) + 2\mu(\Xi_b^{0'*}) \\
\mu(\Sigma_b^{-*}) + 2\mu(\Xi_b^{-'*}) &= 3\left(\mu(\Sigma_b^-) + 2\mu(\Xi_b^{0'})\right) \\
\frac{2}{3}\mu(\Sigma_b^{+*}) &= \mu(\Sigma_b^-) + 2\mu(\Xi_b^{0'}) - \mu(\Sigma_b^+) \\
6\mu(\Sigma_b^0) - 4\mu(\Sigma_b^+) &= -4\mu(\Sigma_b^{0*}) + \frac{8}{3}\mu(\Sigma_b^{+*}) \ , \qquad (21)
\end{aligned}$$

and two independent equations that relate b- and c-baryons

$$\begin{aligned}
\mu(\Sigma_b^0) - \mu(\Sigma_b^+) &= \mu(\Sigma_c^+) - \mu(\Sigma_c^{++}) \\
\mu(\Sigma_c^{++}) - \frac{1}{3}\mu(\Sigma_c^{++*}) &= \mu(\Sigma_b^+) - \frac{1}{3}\mu(\Sigma_b^{+*}) \ . \qquad (22)
\end{aligned}$$

Notice also that we can construct other combinations such that c_s, g_2^2 and g_3^2 contributions cancel

$$\begin{aligned}
\mu(\Sigma_c^{++}) + \mu(\Sigma_c^0) + \mu(\Omega_c^0) = \mu(\Sigma_c^+) + \mu(\Xi_c^{0'}) + \mu(\Xi_c^{+'}) &= \frac{1}{6}\frac{\mu_{HQE}(B^{(*)})}{m_c} \\
\mu(\Sigma_b^+) + \mu(\Sigma_b^-) + \mu(\Omega_b^-) = \mu(\Sigma_b^0) + \mu(\Xi_b^{-'}) + \mu(\Xi_b^{0'}) &= -\frac{1}{12}\frac{\mu_{HQE}(B^{(*)})}{m_b} \ . \qquad (24)
\end{aligned}$$

$$\begin{array}{ccccccccccc}
\Sigma_c^{++} & + & \Sigma_c^{0} & + & \Omega_c^{0} & = & \Sigma_c^{+} & + & \Xi_c^{0} & + & \Xi_c^{+} \\
x^4 \cdot t^1 & & x^4 \cdot t^3 & & x^6 \cdot t^3 & & x^4 \cdot t^2 & & x^5 \cdot t^3 & & x^5 \cdot t^2 \\
\hline & \cdot & & \cdot & & = & & \cdot & & \cdot & \\
x^1 \cdot t^3 & & x^1 \cdot t^5 & & x^3 \cdot t^5 & & x^1 \cdot t^4 & & x^2 \cdot t^5 & & x^2 \cdot t^4
\end{array} \qquad \begin{array}{cc} 19 & 20 \\ 19 & 20 \end{array}$$

There exists an experimental measurement of g_3 from CLEO coming from the decay $\Sigma_c^* \to \Lambda_c \pi$ [10, 12], $g_3 = \sqrt{3}\,(0.57 \pm 0.10)$. The direct measurement of g_2 is not possible at

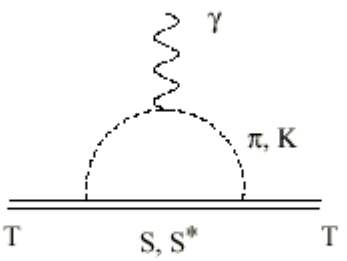

Figure 2: Meson loops contributing to T-baryons MM.

c quark	b quark	μ_T	μ_{g_3}	$\mu_{g'}$	μ_{χ_1}	μ_{χ_2}
Ξ_c^0	Ξ_b^-	4	$J_\pi + J_K$	$I_\pi + I_K$	$-2m_\pi^2/m_K^2$	m_π^2/m_K^2
Ξ_c^+	Ξ_b^0	-2	$-J_\pi$	$-I_\pi$	m_π^2/m_K^2	m_π^2/m_K^2
Λ_c^+	Λ_b^0	-2	$-J_K$	$-I_K$	$2 - m_\pi^2/m_K^2$	$2 - m_\pi^2/m_K^2$

Table 4: Contributions to magnetic moments of spin 1/2 T-baryons ($s_l = 0$).

$$m_b\,\mu(\Xi_b^-) - m_c\,\mu(\Xi_c^0) = m_b\,\mu(\Xi_b^0) - m_c\,\mu(\Xi_c^+) \quad (35)$$

$$m_b\,\mu(\Lambda_b^0) - m_c\,\mu(\Lambda_c^+) - \frac{1}{4} = \left(2\frac{m_K^2}{m_\pi^2} - 1\right)\left[m_b\,\mu(\Xi_b^-) - m_c\,\mu(\Xi_c^0) - \frac{1}{4}\right] . \quad (36)$$

$$\Xi_b^- - \Xi_c^0 = \Xi_b^0 - \Xi_c^+ \qquad \frac{x^4 \cdot t^1}{x^1 \cdot t^3} \cdot \frac{x^5 \cdot t^3}{x^2 \cdot t^5} = \frac{x^4 \cdot t^3}{x^1 \cdot t^5} \cdot \frac{x^5 \cdot t^2}{x^2 \cdot t^4} \qquad 19\ \ 20$$

TABLE I. Predictions of different models for charmed baryons electromagnetic mass splittings

Model	$\Sigma_c^{++} - \Sigma_c^0$	$\Sigma_c^+ - \Sigma_c^0$	$\Xi_c^0 - \Xi_c^+$
Coulomb electric interaction. Here we use the model AL1.			

Baryons	Δm	ΔT	ΔW	ΔB	ΔC	Total
$n - p$	11	0.33	–6.45	–2.86	–0.76	1.24
$\Sigma_c^+ - \Sigma_c^0$	–11	0.56	7.55	1.39	1.14	–0.35
$\Sigma_c^{++} - \Sigma_c^0$	–22	0.79	15.78	2.07	4.53	1.20
$\Xi_c^0 - \Xi_c^+$	11	–3.31	–5.56	1.72	–1.01	2.83

TABLE III. Comparison of the isospin-breaking splittings of mesons (in MeV) obtained from several potential models: Bhaduri et al. (BCN); Silvestre-Brac and Semay (AL1 with linear confinement, AP1 with a $r^{2/3}$ confinement).

Splitting	Exp. (Ref. [6])	BCN	AL1	AP1
$K^0 - K^+$	3.995 ± 0.034	13.15	6.64	9.56
$K^{*0} - K^{*+}$	6.7 ± 1.2	1.55	1.36	1.28
$D^+ - D^0$	4.78 ± 0.10	5.37	3.78	–0.33
$D^{*+} - D^{*0}$	2.6 ± 1.8	2.44	2.74	–0.16
$B^0 - B^-$	0.35 ± 0.29 [1]	–1.46	–1.29	–6.06
$B^{*0} - B^{*-}$		–2.04	–1.23	–5.26

TABLE IV. Comparison of the isospin-breaking splittings (in MeV) obtained from several potential models: Bhaduri et al. (BCN); Silvestre-Brac and Semay (AL1 with linear confinement, AP1 with a $r^{2/3}$ confinement); Richard and Taxil where the hyperfine interaction is treated perturbatively (RT II has a linear central potential, RT I a $r^{0.1}$ one). In the column AL1 + dd, the magnetic dipole–dipole interaction between quarks is accounted for, in addition to the electrostatic potential. Some redundant splittings are shown for the ease of discussion.

Splitting	Exp. [Ref]	BCN	AL1	AP1	RT II	RT I	AL1 + dd
$n-p$	1.293318± 0.0000009 [6]	1.38	1.16	1.29	1.2	1.3	1.24
$\Delta^+ - \Delta^{++}$		0.54	0.08	2.08			0.36
$\Delta^0 - \Delta^{++}$	2.7 ± 0.3 [6]	3.21	2.20	6.10			2.54
$\Delta^- - \Delta^{++}$		8.04	6.34	11.38			6.55
$\Sigma^- - \Sigma^0$	4.88 ± 0.08 [6]	7.09	5.16	6.07	2	4	5.24
$\Sigma^- - \Sigma^+$	8.09 ± 0.16 [6]	11.98	8.25	10.57	4	7	8.67
$\Sigma^{*0} - \Sigma^{*+}$	–4 to 4 [6]	4.10	1.82	2.65	4	6	1.96
$\Sigma^{*-} - \Sigma^{*0}$	2.0 ± 2.4 [6]	6.34	3.85	4.40	3	4	3.69
$\Xi^- - \Xi^0$	6.4 ± 0.6 [6]	10.62	7.12	9.19	3	6	7.46
$\Xi^{*-} - \Xi^{*0}$	3.2 ± 0.6 [6]	5.87	3.68	3.58	3	3	3.58
$\Sigma_c^{++} - \Sigma_c^0$	0.8 ± 0.4 [6]	0.12	1.06	2.91	–2	3	1.20
$\Sigma_c^+ - \Sigma_c^0$	1.4 ± 0.6 [6]	–0.96	–0.55	0.55	–2	1	–0.36
$\Xi_c^0 - \Xi_c^+$	$2.5 \pm 1.7 \pm 1.1$ [18]	4.67	2.58	2.90	2	0	2.83
$\Xi_c'^0 - \Xi_c'^+$	1.7 ± 4.6 [18]	1.04	0.47	–0.22	1	0	0.30
$\Xi_c^{*0} - \Xi_c^{*+}$	6.3 ± 2.6 [18]	0.40	0.44	-0.85	1	0	0.43
$\Sigma_b^+ - \Sigma_b^-$		–3.58	–3.45	5.64			–3.57
$\Sigma_b^0 - \Sigma_b^-$		–2.85	–1.99	0.01			–2.51
$\Xi_b^- - \Xi_b^0$		7.25	5.12	4.27			5.39
$\Xi_{cc}^+ - \Xi_{cc}^{++}$	-1.87	-2.70	-5.21				-2.96
$\Sigma_c^{++} - \Sigma_c^+$		1.08	1.61	2.36	0	2	1.56
$\Sigma^+ + \Sigma^- - 2\Sigma^0$		2.20	2.07	1.57			1.81
$\Sigma^{*+} + \Sigma^{*-} - 2\Sigma^{*0}$		2.24	2.03	1.75			1.73
$\Sigma_c^{++} + \Sigma_c^0 - 2\Sigma_c^+$		2.04	2.16	1.81			1.92

velká pyramida uuu až ttt mreece@midway.uchicago.edu mreece@midway.uchicago.edu *poslal

(3) 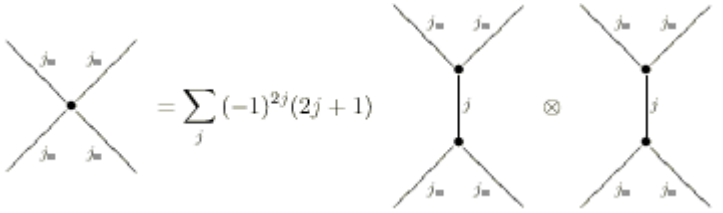

where we sum over spins j such that the triples j_1, j_2, j and j_3, j_4, j are both admissible.

In terms of balanced spin networks, the face, edge and vertex amplitudes of the DFKR model are given as follows:

$A(f)$ = 

$A(e)$ = 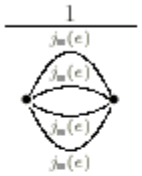

(4) $A(v)$ = 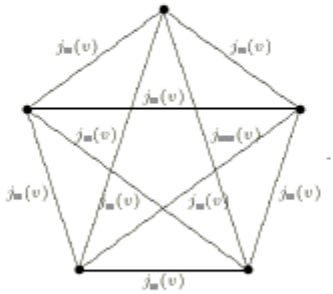

Here the intertwiner in the first spin network is just the identity operator, so the face amplitude $A(f)$ is just the dimension of the representation $j(f) \otimes j(f)$, that is, $(2j(f)+1)^2$. The '$4j$ symbol'

in a triangular spin-$\frac{1}{2}$ loop in four of the $10j$ symbols. Since

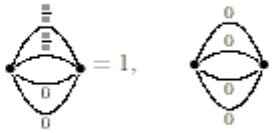

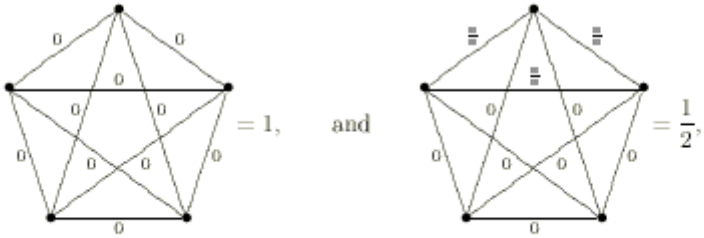

each spin foam of this sort contributes an amplitude of $2^{-16} \cdot (\frac{1}{2})^4 = 2^{-20}$. There are

The LSND experiment [30] has studied neutrinos from
opped positively-charged pions, which decay via the chain

$$\pi^+ \to \mu^+ \nu_\mu$$
$$\hookrightarrow e^+ \nu_e \overline{\nu}_\mu \qquad (22)$$

$$\pi^+ \to \mu^+ \nu_\mu \qquad (23)$$

$$\pi^+ = \mu^+ + \nu_\mu$$
$$\mu^+ = e^+ + \nu_e + \overline{\nu}_\mu$$

$\pi^+ = \mu^+ + \nu_\mu$

$\mu^+ = e^+ + \nu_e + \nu_{\mu^-}$

$$\frac{x.t}{x.t} = \frac{x.t}{x.t} \cdot \frac{x.t}{x.t}$$

$$\frac{x.t}{x.t} = \frac{x.t}{x.t} \cdot \frac{x.t}{x.t} \cdot \frac{x.t}{x.t}$$

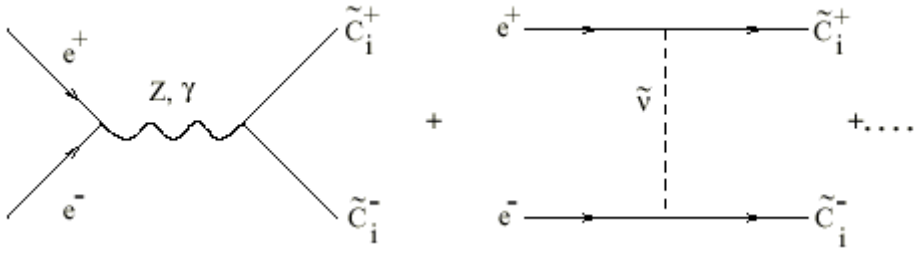

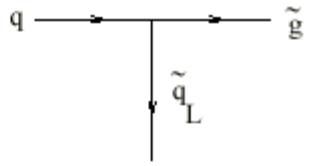

$-ig_3 G^* \frac{1-\gamma_5}{\sqrt{2}}$

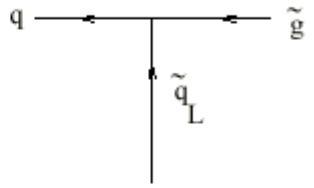

$-ig_3 G \frac{1+\gamma_5}{\sqrt{2}}$

not including the color factors.

Now consider gluino production $q + \bar{q} \to \tilde{g} + \tilde{g}$. Factors of G and G^* enter so that there is no dependence on the phase from these two diagrams.

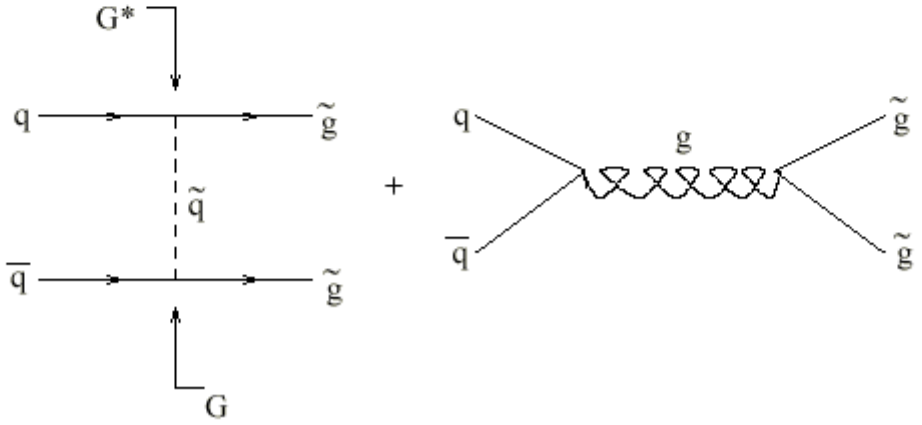

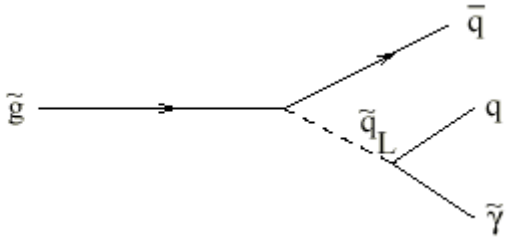

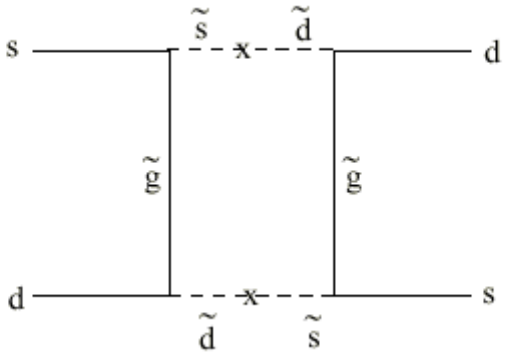

For ε'/ε the same sparticles enter in the penguin diagram,

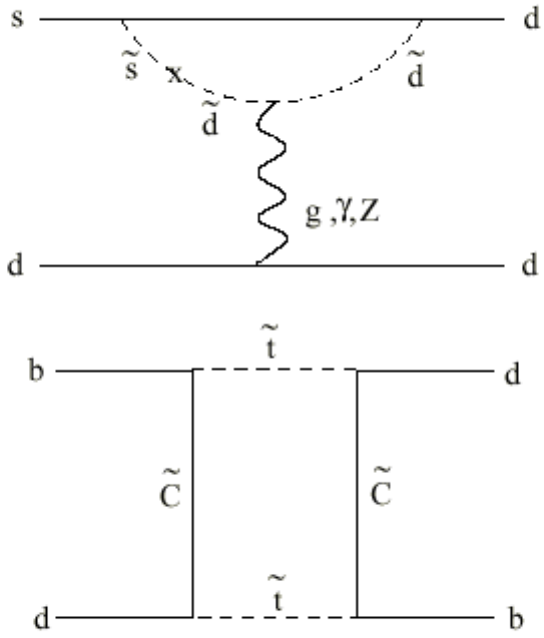

and the phases $\phi_2, \phi_\mu, \phi_{A_\ell}$ enter at the vertices. With our assumptions we predict (sin 2α and sin 2β are defined to be the CP asymmetries measured in the decays $B_d \to \pi^+\pi^-$ and ψK_s)

quark distributions at $x = 1 - m_v/m_{\Sigma^*} = 1 - 850/1385 \approx 0.39$. The quark distributions, for example, for the Σ^{*+} are given by the same expressions as those for Δ^+ replacing d by s and noting that the u distribution is to be calculated with the heavy diquark masses and the s distribution using the light diquark masses. Further, note that we have $\Delta q^{\frac{3}{2}}(x) \equiv q^{\Uparrow}(x) - q^{\Downarrow}(x) = 3\Delta q^{\frac{1}{2}}(x) \equiv q^{\uparrow}(x) - q^{\downarrow}(x)$. In Figs. 8 and 9 we show the unpolarized and polarized quark distributions in the Δ^+ and Σ^{+*}. The Δq are for the spin-$\frac{1}{2}$ projections. They have to be multiplied by 3 to obtain the corresponding distributions for the spin-$\frac{3}{2}$ projections. In Fig. 4, we show the ratio $r_{\Sigma^*} \equiv s_{\Sigma^*}/u_{\Sigma^*}$ compared to the corresponding ratios in other hyperons.

discussed in more detail in Ref. [28], the meson-cloud predicts an excess of $\bar{d}$ over $\bar{u}$ in Σ^+ hyperons similar to that in observed in protons, while SU(3) suggests $\bar{d} < \bar{u}$, since under $p \leftrightarrow \Sigma^+$ we have $s(\bar{s}) \leftrightarrow d(\bar{d})$. The meson-cloud also modifies the bare quark distributions

$$
\begin{aligned}
&\Sigma^+(uus) \to \Lambda^0(uds)\,\pi^+(u\bar{d}) \\
&\Sigma^+(uus) \to \Sigma^0(uds)\,\pi^+(u\bar{d}) \\
&\Sigma^+(uus) \to \Sigma^+(uus)\pi^0(\frac{1}{\sqrt{2}}[d\bar{d}-u\bar{u}]) \\
&\Sigma^+(uus) \to \Sigma^{0*}(uds)\,\pi^+(u\bar{d}) \\
&\Sigma^+(uus) \to \Sigma^{+*}(uus)\,\pi^0(\frac{1}{\sqrt{2}}[d\bar{d}-u\bar{u}]) \\
&\Sigma^+(uus) \to p(uud)\,\bar{K}^0(\bar{d}s).
\end{aligned} \tag{20}
$$

The corresponding lowest fluctuations for the proton are

$$
\begin{aligned}
&p(uud) \to n(udd)\,\pi^+(u\bar{d}) \\
&p(uud) \to p(uud)\,\pi^0(\frac{1}{\sqrt{2}}[d\bar{d}-u\bar{u}]) \\
&p(uud) \to \Delta^+(uud)\,\pi^0(\frac{1}{\sqrt{2}}[d\bar{d}-u\bar{u}]) \\
&p(uud) \to \Delta^0(udd)\,\pi^+(u\bar{d}) \\
&p(uud) \to \Delta^{++}(uuu)\,\pi^-(\bar{u}d).
\end{aligned} \tag{21}
$$

Since the Δ plays an important role in the nucleon, we also include the $\Sigma^*\pi$ components of the wave function in the Σ^+ case.

In deep inelastic scattering, the virtual photon can hit either the bare hadron, H, or one of the constituents of the higher Fock states. In the infinite momentum frame, where the

10

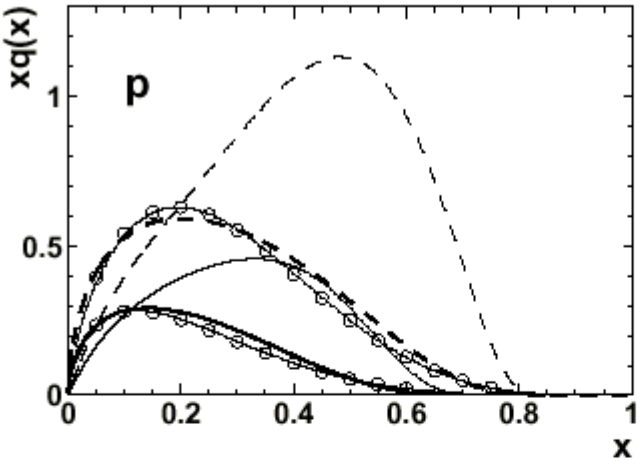

FIG. 1. The up (dashed lines) and down (solid lines) valence quark distribution in the proton at $Q^2 = \mu^2 = 0.23$ GeV^2 (light lines) and $Q^2 = 10$ GeV^2 (heavy lines). The quark distributions at $Q^2 = 10$ GeV^2 already include the meson-cloud corrections. The Cteq4M distributions representing the "data" are shown as solid lines with open circles.

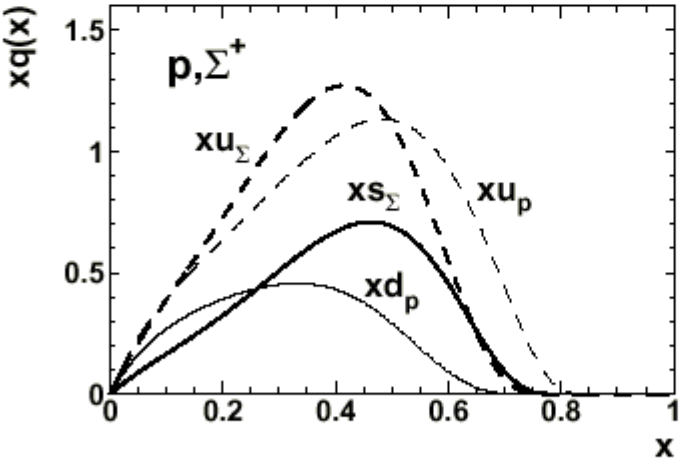

FIG. 2. The strange (heavy solid line) and up (heavy dashed line) valence quark distributions in Σ^+ compared to the down (light solid line) and up (light dashed line) quark distributions in the proton – all evaluated at the bag scale, μ^2.

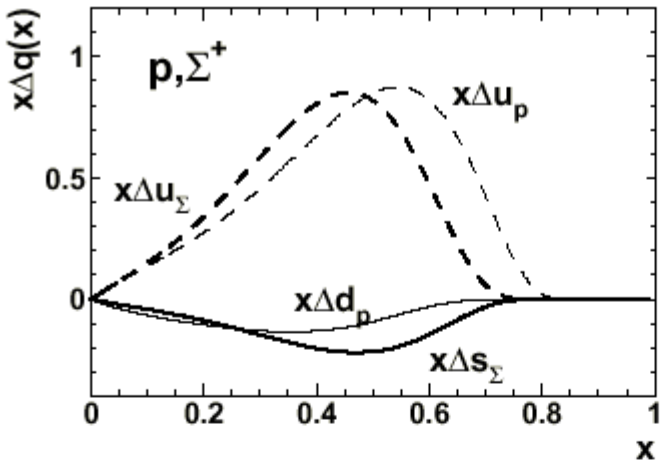

FIG. 3. The polarized strange $x\Delta s(x) = xs^{\uparrow}(x) - xs^{\downarrow}(x)$ (heavy solid line) and up $x\Delta u(x)$ (heavy dashed line) valence quark distributions in the Σ^+, compared to the polarized down (light solid line) and up (light dashed line) quark distributions in the proton (at the bag scale, μ^2).

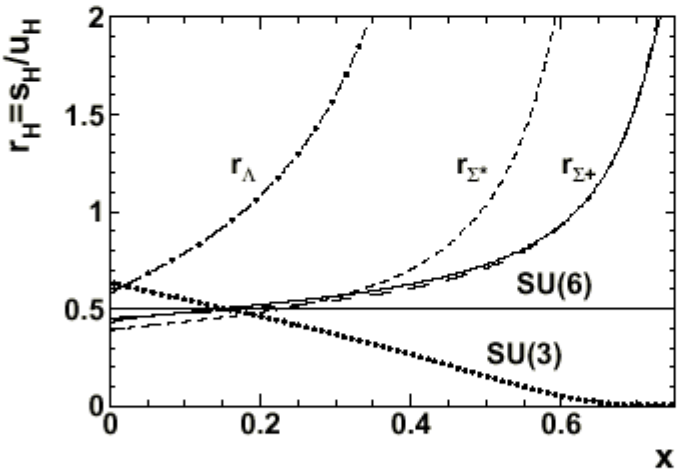

FIG. 4. The ratios $r_H \equiv s_H/u_H$ for different baryons, after evolving the quark distributions to $Q^2 = 10$ GeV^2. The ratio $r_{\Sigma^+} \equiv s_{\Sigma^+}/u_{\Sigma^+}$ is shown as the solid and dashed lines, with and without meson-cloud corrections, respectively. The $SU(3)$ expectation, which corresponds to $r_\Sigma = \frac{1}{2}r_\Lambda = r_p = d_p/u_p$, is shown as a dotted line. $SU(6)$ would give a constant ratio of $1/2$, independent of x (solid line), and is realized for the decuplet baryons containing only massless quarks (Δ^+). However, it is broken for the decuplet hyperons (short dashed line) – see sec. IIB.

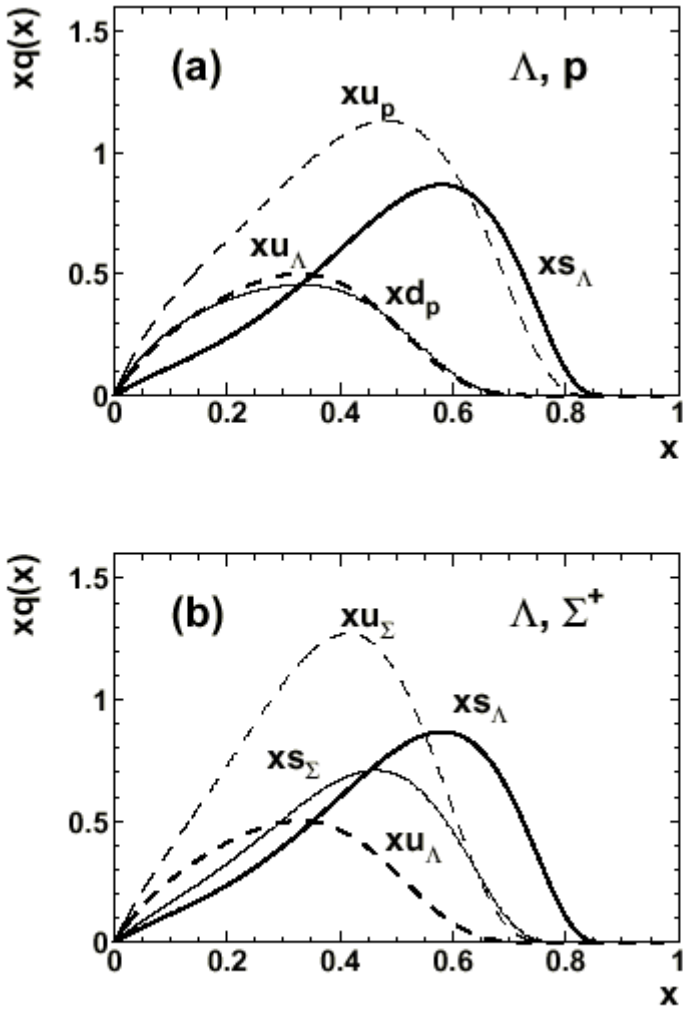

FIG. 5. Quark distributions in the Λ compared to the quark distribution (a) in the proton and (b) in the Σ^+ – at the bag scale, μ^2.

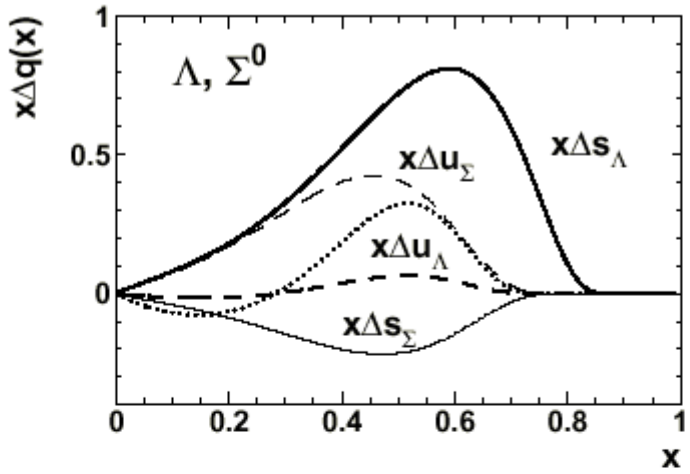

FIG. 6. Polarized quark distributions in the Σ^0 and the Λ at the bag scale, μ^2. The dotted line stands for five times $x\Delta u_\Lambda$ and indicates the relative importance of the u and d quarks in g_1.

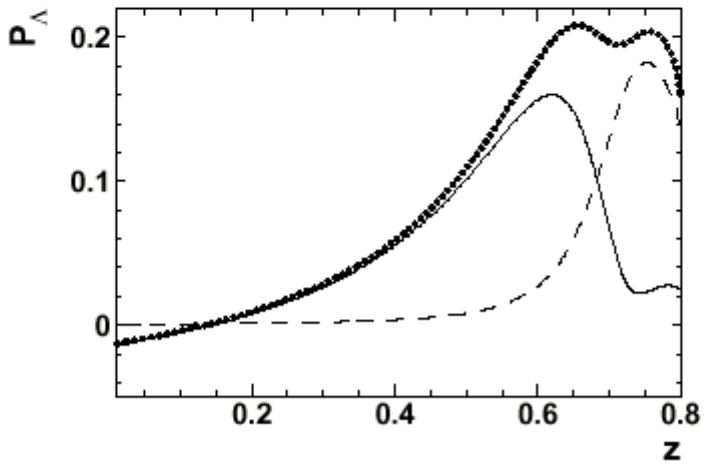

FIG. 7. The polarization of the Λ produced in semi-inclusive, polarized $e-p$ scattering, with the electron polarization arbitrarily set to 50%. The contributions from the fragmentation of u and s quarks are shown as solid and dashed lines, respectively. The dotted line is the total polarization.

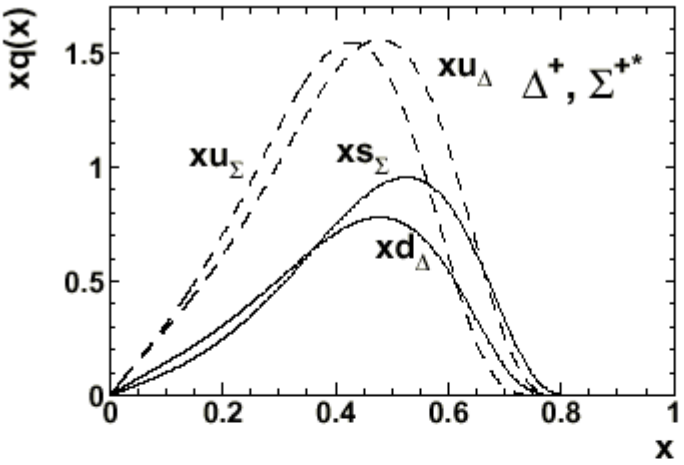

FIG. 8. Quark distributions in the Δ^+ and Σ^{+*} at the bag scale, μ^2.

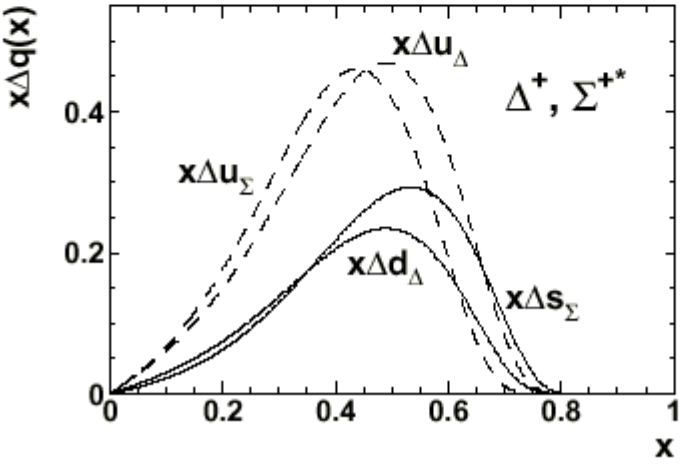

FIG. 9. Polarized quark distributions in the Δ^+ and Σ^{+*} at the bag scale, μ^2.

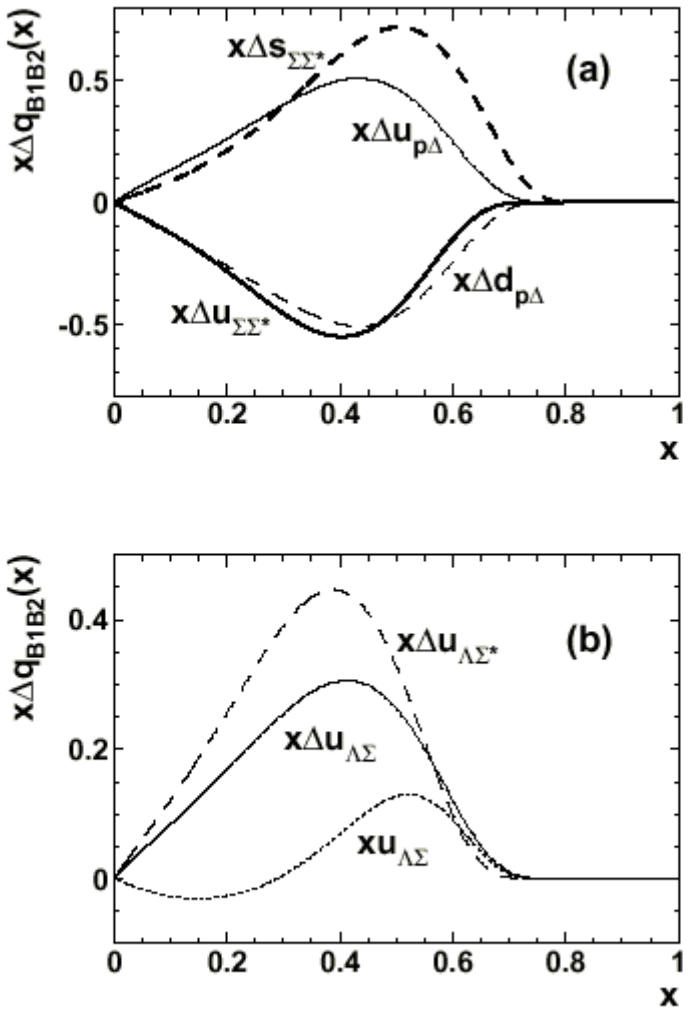

FIG. 10. Interference distributions as calculated in the MIT bag at the scale, μ^2. (a) N-Δ and Σ-Σ^* interference terms; (b) Λ-Σ and Λ-Σ^* intereference terms. The d distributions have the same magnitude but opposite signs than the corresponding u-distributions.

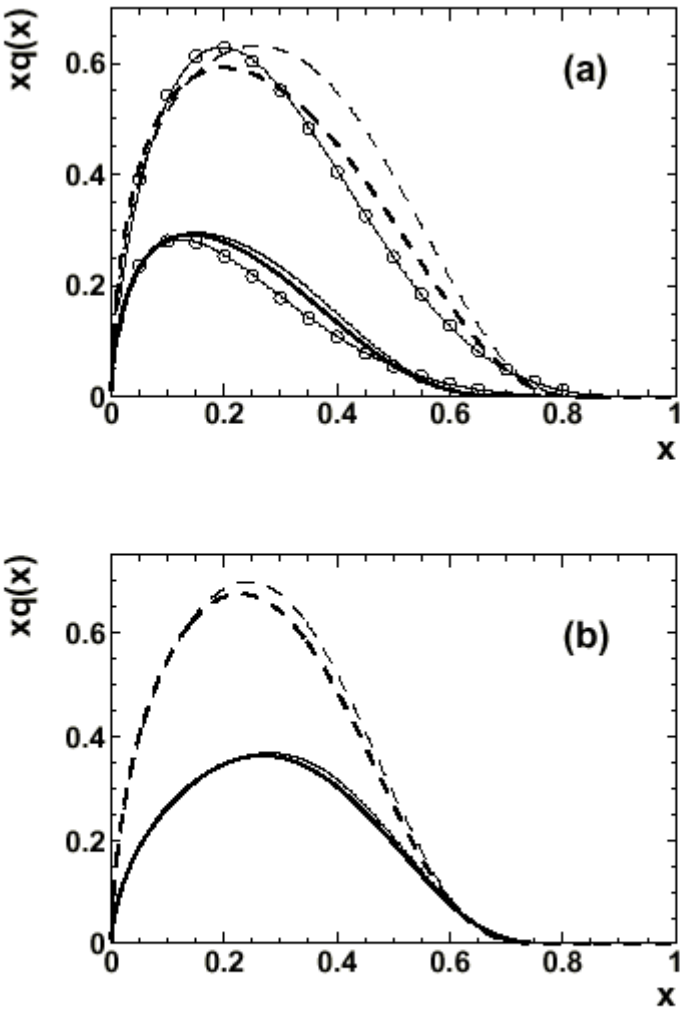

FIG. 12. (a) The up (dashed lines) and down (solid lines) valence quark distribution in the proton without (light lines) and with (heavy lines) meson-cloud corrections at $Q^2 = 10$ GeV^2. The Cteq4M distributions representing the "data" are shown as solid lines with open circles. (b) The up (dashed lines) and strange (solid lines) valence quark distribution in the Σ^+ without (light lines) and with (heavy lines) meson-cloud corrections at $Q^2 = 10$ GeV^2.

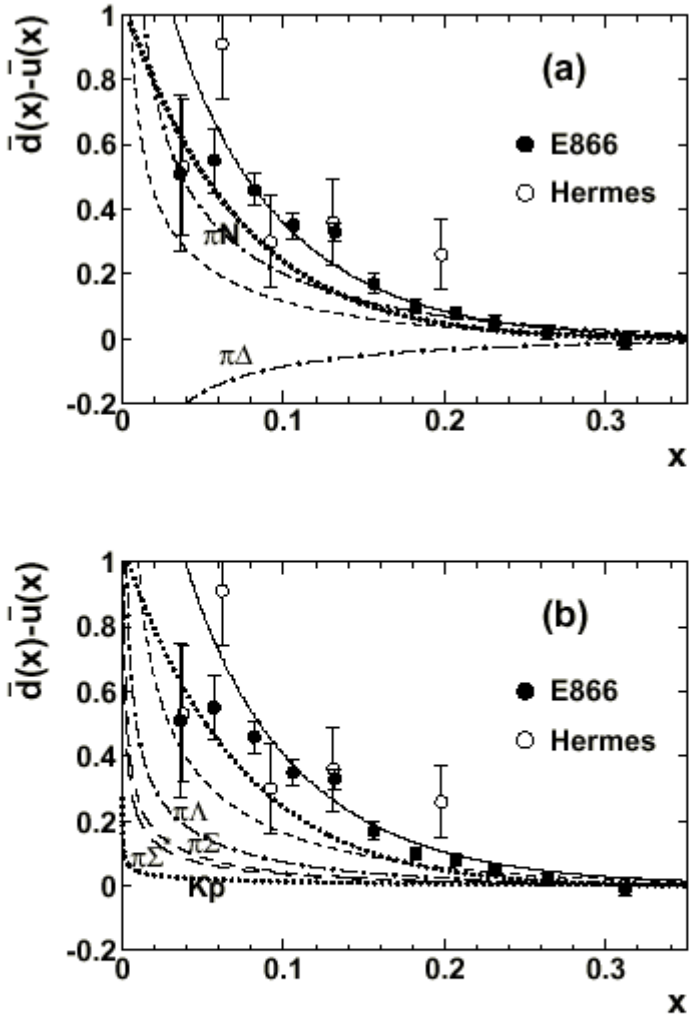

FIG. 13. Flavor symmetry violation, $\bar{d}-\bar{u}$, for (a) the proton and (b) the Σ^+. In the proton case, the upper and lower dash-dotted lines stand for the πN and $\pi\Delta$ contributions alone and the dashed line for their sum. The data are taken from Refs. [17,18]. In the Σ^+ case, the upper and lower dashed lines stand for the $\pi\Sigma$ and $\pi\Sigma^*$ contributions, the dotted line for the Kp and the dash-dotted line for the $\pi\Lambda$ contributions – and the proton data is shown just to set the scale. The short dashed line is the sum of the chiral components. The dotted lines are the Pauli contributions and the solid lines stand for the total FSV.

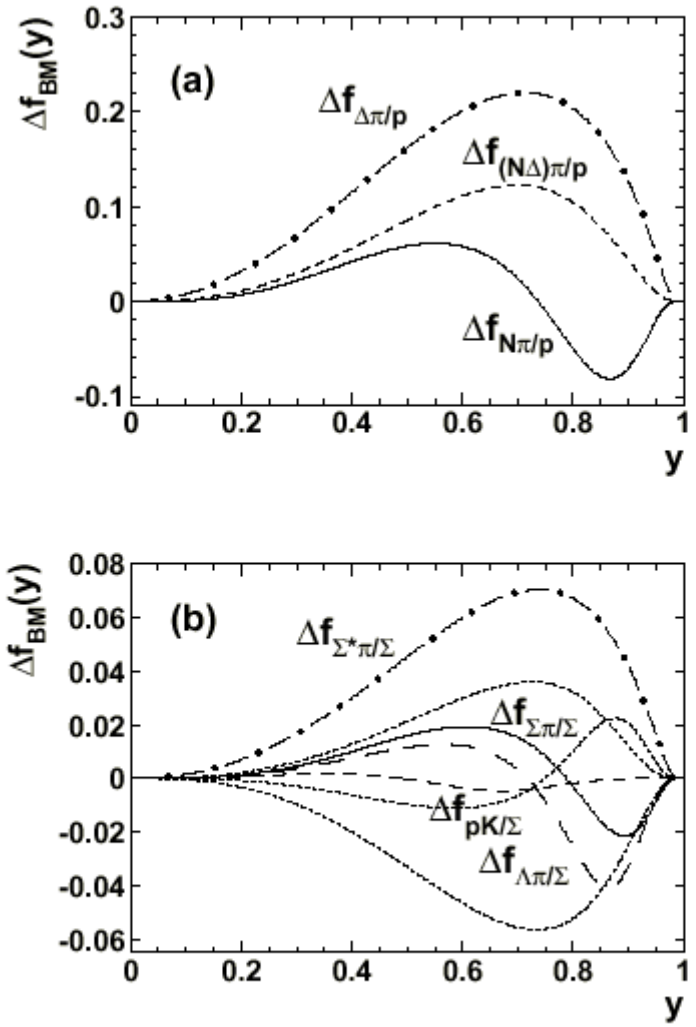

FIG. 14. The polarized splitting functions for the transitions (a) $p \to BM$ and (b) $\Sigma^+ \to BM$. The dotted lines are the interference splitting functions; $\Delta f_{(\Lambda\Sigma^*)\pi/\Sigma}$ (upper line), $\Delta f_{(\Lambda\Sigma)\pi/\Sigma}$ (middle line) and $\Delta f_{(\Sigma\Sigma^*)\pi/\Sigma}$ (lower line).

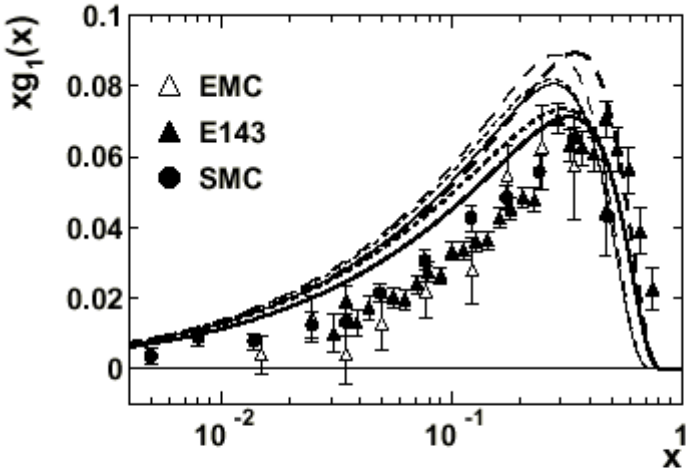

FIG. 15. g_{1p} with (light solid line) and without (light dashed line) meson-cloud corrections compared to the corresponding $g_{1\Sigma^+}$ in the proton (heavy lines). The data are for the proton and taken from Refs. [33–35]. The structure functions calculated with interference terms are shown as short dashed lines. The EMC data are at different Q^2 values, the SMC at $Q^2 = 10$ GeV^2 and the E143 data at $Q^2 = 5$ GeV^2.